# Miniature time-of-flight mass analyzer for use in combination with a compact highly-repetitive femtosecond laser ionization source

Yoshinaga, Katsunori
Faculty of Design, Kyushu University

Hao, Nguyen V.
Center of Future Chemistry, Kyushu University

Imasaka, Totaro
Center of Future Chemistry, Kyushu University

Imasaka, Tomoko
Faculty of Design, Kyushu University



出版情報：Analytica Chimica Acta. 1203, pp.339673-, 2022-04-22. Elsevier
バージョン：
権利関係：

# Miniature time-of-flight mass analyzer for use in combination with a compact highly-repetitive femtosecond laser ionization source

**Katsunori Yoshinaga [a], Nguyen V. Hao [b], Totaro Imasaka [b, c, d], Tomoko Imasaka [a, *]**

[a]*Faculty of Design, Kyushu University, 4-9-1, Shiobaru, Minami-ku, Fukuoka 815-8540: 744 Motooka, Nishi-ku, Fukuoka 819-0395, Japan*

[b]*Center of Future Chemistry, Kyushu University,744 Motooka, Nishi-ku, Fukuoka 819-0395, Japan; Present address, Institute of Science and Technology, TNU - University of Sciences, Tan Thinh ward, Thai Nguyen City, Vietnam*

[c]*Kyushu University,744 Motooka, Nishi-ku, Fukuoka 819-0395, Japan*

[d]*Hikari Giken, Co., 2-10-30, Sakurazaka, Chuou-ku, Fukuoka 810-0024, Japan*

* Corresponding author.

*Email address*: imasaka@design.kyushu-u.ac.jp (Tomoko Imasaka).

**ABSTRACT**

In most cases, a molecular ion is observed in femtosecond laser ionization mass spectrometry, which provides information concerning the molecular weight of the analyte. However, the Ti:sapphire laser currently used as the ionization source is costly and involves special skills for operation and maintenance, which prevents its practical use in many applications. In this study, we report on the development of a miniature time-of-flight mass analyzer with a flight tube length of 65 mm for use in combination with a compact highly-repetitive (120-560 kHz) femtosecond Yb laser and a time-correlated single ion counting system. The fundamental beam (1030 nm) was converted into ultraviolet beams emitting at 343, 257, and 206 nm, which was utilized as an efficient two-photon ionization source. A mass resolution of 670 was achieved for the molecular ion of chlorobenzene, the minimum time for measuring a mass spectrum being 0.1 s. This mass spectrometer was used in the on-site real-time monitoring of products appeared by the combustion of plastic, some nerve agent analogs, and an explosive in the air. The interference arising from nitrogen and oxygen in the air was suppressed, since they require nonresonant four- and three-photon ionizations, respectively. The mass spectrometer was combined with a gas chromatograph and used for the comprehensive analysis of polycyclic aromatic hydrocarbons, suggesting its potential advantage for use in the practical trace analysis of organic compounds in the environmental and forensic sciences.

Keywords: femtosecond ionization, miniature mass analyzer, time-correlated single ion counting, mass spectrometry, gas chromatograph detector

## 1. Introduction

Mass spectrometry (MS) has become an essential tool for the trace analysis of organic compounds because of its excellent performance in terms of sensitivity and selectivity [1]. When used in combination with a separation technique such as gas chromatography (GC), numerous constituents in a complex matrix can be determined with minimal pretreatment procedures, thus providing an indispensable tool for use in academic and industrial institutions. In this technique, a molecule is usually ionized by an electron, and is referred to as electron ionization mass spectrometry (EIMS). This technique is simple and cost-effective, and is widely used in numerous applications. However, the elastic collision of electrons makes it difficult to control the ionization process. As a result, various fragment ions are produced, making the observation of a molecular ion and the subsequent determination of a molecular weight difficult. Several techniques have been developed to date to overcome this problem, including chemical ionization, laser desorption ionization (LDI), electrospray ionization, and matrix-assisted laser desorption ionization (MALDI) [2-4]. However, these methods all have their advantages and disadvantages, depending on the application.

Photoionization is successfully used for soft ionization since the energy remaining in the ionic state can be controlled by changing the photon energy, i.e., the wavelength of a light source, which suppresses the fragmentation of the molecular ion. The ionization energy of most organic compounds is 7-15 eV, and a vacuum ultraviolet light source can be used for single-photon ionization [5-7]. A pulsed laser has been employed for multiphoton ionization (MPI), which can be combined with a time-of-flight mass spectrometer (TOFMS) and then used in a comprehensive analysis [8,9]. In this approach, an analyte molecule is excited by absorbing the first photon and is subsequently ionized by absorbing the second photon, a process that is referred to as resonance-enhanced two-photon (or multiphoton) ionization (RE2PI or REMPI), providing spectral selectivity in mass spectrometry. When the analyte molecule has a short excited-state lifetime by the substitution of a hydrogen atom with chlorinated/brominated or nitrated groups, the use of a femtosecond laser is preferred [10-13]. This method is particularly useful when the electronic excited state is located at above half of the ionization energy (*IE*) and non-resonant two-photon ionization (NR2PI) must then be used to reduce the excess energy, in which the laser wavelength can be adjusted to the half value of the *IE* to minimize excess energy [14]. In fact, a variety of organic compounds including pesticides, explosives, and allergenic compounds with flexible side chains have been determined, since this method largely provides molecular ions [15]. A spectrally-chirped femtosecond pulse has been successfully used for discriminating the structural isomers of difluorobenzene and fluorotoluene [16,17]. Alternatively, a

pump-probe technique can be employed to measure a transient decay curve with an interference pattern for discriminating the isomers of nitrotoluene [18-20].

Despite the superior performance of femtosecond ionization mass spectrometry (fs-LIMS), it is not used extensively in practical trace analysis, since the Ti:sapphire laser (TS) used as the ionization source requires high capital and running costs and special skills for the operation and maintenance. An optical parametric amplifier pumped by a TS has been employed as a tunable ionization source, the wavelength of which is further converted from the near-infrared (NIR) into the ultraviolet (UV) region using a series of nonlinear optical phenomena such as harmonic generation and frequency mixing [15]. Because of this, the analytical system is quite complicated. It should be noted that the TS is typically operated at 1 kHz and the beam diameter is expanded to ca. 0.5 mm in the ionization region to reduce photon density so as to avoid serious fragmentation and signal saturation. The speed of a molecule at room temperature is ca. 100 m/s, and only a small portion of the molecules (0.005 = 0.5 mm × 1 kHz/100 m/s) is irradiated by a laser pulse and then ionized for mass analysis. Because of this, the ionization efficiency of the analyte is limited to 0.5%, as a maximum. As a result, it would be desirable to use a laser that can be operated at a higher repetition rate (e.g., 1 MHz) to approach a nearly 100% ionization efficiency.

A new type of laser based on optical fiber technology has been developed for scientific and industrial applications. In this case, a laser-active medium in the optical fiber is directly pumped by a diode laser, thus reducing size/cost and improving ruggedness/stability. In fact, a recently developed femtosecond Yb laser has been utilized for material processing, e.g., cutting and welding of a steel plate and for manufacturing various displays made of inorganic/organic glass. It can also be used in spectrometric applications, because of its high efficiency, large output power, compactness, high-stability, low-cost, and capability of turn-key operation without maintenance. These favorable properties would permit practical use of the laser as the ionization source in MS. However, this type of laser is operated at a high repetition rate (e.g., 27 MHz) in the oscillator stage, which is determined by the cavity length, i.e., the round trip time in the optical fiber. In order to decrease the pulse repetition rate and to increase the pulse energy, a series of pulses is picked up periodically and then amplified in the next optical fiber typically at ca. 1-27 MHz, which can be further amplified in a larger-core fiber at ca. 0.1-1 MHz. The pulse can be amplified to milli-joule levels at several kHz in a multi-pass disk amplifier, although the optical system becomes more complicated. Therefore, the use of a laser at ca. 1-27 MHz (one fiber amplifier) or ca. 0.1-1 MHz (two fiber amplifiers) would be highly desirable for practical use.

There is a problem that needs to be solved for such a highly-repetitive laser source to be used in MS, in that the time resolution and the maximum recording rate of a digitizer used for measuring the mass spectrum is limited to 1 ns and 20-100 kHz, respectively. It should be noted that a mass spectrum can be measured by constructing a histogram of the time interval between the laser pulse and the single ion pulse, as in the case of time-correlated single "photon" counting (TCSPC) used for recording a fluorescence decay curve to measure the lifetime of the excited state. This TCSPC technique is widely used because of its high sensitivity based on photon counting and the high time resolution that is not determined by the response time but, rather, is determined by a transient time spread of the detector. Even a picosecond decay curve can be measured accurately with excellent sensitivity. Due to the short fluorescence lifetime (typically, <10 ns) of an organic compound, a highly-repetitive light source (e.g., 27 MHz) is preferable, since it allows the number of photons counted to be increased, thus reducing shot noise, which improves the accuracy of the measurement. Similarly, an optical-fiber-based laser can be used for time-correlated single "ion" counting (TCSIC) in TOFMS. However, the flight time of the ion is typically 30 μs (or longer in high-resolution MS) [15], requiring a laser operated at <0.03 MHz. When a laser operated at 1 MHz is used as the ionization source, the mass spectra are overlapped with respect to each other. To address this issue, a miniature TOF mass analyzer needs to be developed, since the flight time can be reduced to <10 μs (preferentially to <1 μs). However, a recent trend involves increasing the flight time to improve the mass resolution, e.g., multi-turn/spiral TOFMS or orbitrap/Fourier-transform MS [21].

A miniature TOF mass analyzer was developed for the use in MS based on LDI and MALDI in 1995-2010, which was accelerated by the Applied Physics Lab TinyTOF program in the USA [22]. For example, an end-cap reflectron MS (reflectron depth 16-34 mm, drift region 4-30 mm) was combined with a nitrogen laser (337 nm, typically 4 ns, 10 Hz) and a digitizer (1-2 G sample/s). By applying a high potential (800-4400 V) for ion acceleration, the flight time could be reduced to 1.2-2.6 μs [22-24]. A linear-type TOF mass analyzer (flight tube 77 mm, 12 kV, 10-20 μs) was developed for measuring high-mass proteins, and the mass resolution was improved to 600-1200 by using a two-stage pulsed-extraction design [25-27]. A highly miniaturized TOFMS (size 53-200 mm, weight 280 g, mass resolution 180) was developed for the planetary mission to measure elements, inorganic salts, and an organic compound of pyrene, in which a Nd:YAG laser (1064-266 nm, 0.66 ns, 7 kHz) was used as the ionization source [28,29]. A TCSIC system combined with a nitrogen laser (4 ns, 10 Hz) was employed for measuring proteins (flight time 25-42 μs) [30]. In addition, a short mass analyzer (flight tube 120 mm, 4 μs) was combined with an optical parametric oscillator pumped by a Nd:YAG laser (6 ns, 10 Hz) for measuring organic compounds in the gas-phase in a supersonic jet [31,32]. In our previous study, we reported on the use of a femtosecond TS (267 nm, 100 fs, 1 kHz) as the

ionization source in a twin-type TOF mass analyzer (flight tube length 64 and 420 mm) using a digitizer and a time-to-amplitude converter combined with a multichannel analyzer. The mass resolution achieved was 450-490 and 900-910 for the MS with the short and long flight tubes, respectively, and the resolution was nearly independent of the electronics used for the signal measurement [33].

In this study, we evaluated the use of a compact highly-repetitive (120-560 kHz) femtosecond Yb laser, the wavelength of which was converted from the NIR into the UV region (206, 257, 343 nm) by nonlinear optical effects based on harmonic generation. A miniature TOF mass analyzer was developed for use in combination with the highly-repetitive UV femtosecond ionization source. The signal was measured by a time-to-digital converter for TCSIC to improve the time resolution and to suppress electronic noise. The MS developed herein was applied for the on-site real-time monitoring of products appeared by the incineration of plastic, and nerve agent analogs and an explosive in the air. Due to the high repetition rate of the laser followed by the short time period for measuring a mass spectrum, TOFMS was combined with GC for the comprehensive analysis of a sample mixture containing 16 polycyclic aromatic hydrocarbons (PAHs). To our knowledge, this is the first report of the development of a TOFMS system comprised of a miniature mass analyzer, a highly-repetitive femtosecond Yb laser, and a TCSIC system. The logic representing the advantage of this combination is summarized in Fig. S1 in the Supporting Information.

## 2. Experimental section

### *2.1. Ionization source*

A femtosecond Yb laser (pulse width 400 fs, wavelength 1030 nm, output power 2.4 W, repetion rate 120 kHz-27 MHz, Calmer Laser) was employed as a fundamental beam to generate harmonic emissions. Fig. 1A shows an optical system for the simultaneous generation of the third and fouth harmonic emissions. The height and direction of the fundamental beam was adjusted using two pairs of dichroic mirrors (R = 99.2% at 1030 nm, Optogama). The laser beam was collimated using a pair of a convex lens (focal length 200 mm, SLB-25.4-200PIR1, Sigma-Koki) and a concave lens (-50 mm, SLB-25-50NIR1, Sigma-Koki), which was passed through a nonlinear optical crystal made of β-barium borate (BBO, $\theta$ = 23.4°, thickness 1.5 mm, type I, Castech) for the second harmonic generation (515 nm). In order to compensate for the relative time delay between the fundamental and second harmonic pulses, both beams were passed though a time plate made of calcite (time delay compensator, 250-600 fs, $CaCO_3$, Newlight). The third harmonic emission (343 nm) and the fourth harmonic emission were generated in series using a BBO crystal ($\theta$ = 40°, $\phi$ = 30°, 6 × 6 × 1.4 mm,

type II, Castech) and a BBO crystal ($\theta$ = 50°, $\phi$ = 0°, 6 × 6 × 0.6 mm, type I, Castech), respectively. The fourth harmonic beam was separated by a dichroic mirror (DM1, R>98.5% at 258 nm, HT>95% at 515/1030 nm, 25.4 × 6 mm) and the remaining fundamental and other harmonic emissions were further removed using dichroic mirrors (DM2-DM4). The third harmonic emission was separated and isolated using dichroic mirrors (DM5-DM8, R>99.5% at 343 nm, HT>90% at 515/1030 nm, 25.4 × 3 mm, Eksma). Both DM2 and DM3 were mounted on the same translation stage that was equipped with a micrometer to adjust the time delay between the fourth and third harmonic pulses. The angles of DM3 and DM4 were adjusted so as to collinearly align the fourth harmonic beam to the third harmonic one. When only the third harmonic emission was used, DM1 and DM4 were removed to reduce the loss at the surface of the optical components. When only the fourth harmonic emission was used, the beam path of the third harmonic emission was interrupted.

Fig. 1B shows the optical system used for simultaneously generating the fourth and fifth harmonic emissions. The BBO crystal for the third harmonic generation was replaced with the BBO crystal for the fourth harmonic generation, and a BBO crystal for the fifth harmonic generation ($\theta$ = 54.3°, $\phi$ = 0°, 6 × 6 × 0.3 mm, type I, Castech) was set at the position of the BBO crystal for the fourth harmonic generation. The fifth harmonic emission was isolated using DM1-DM4 (R>92% at 206 nm, HT>90% at 258/1030 nm, 25.4 × 0.2 mm, Eksma) and was combined with the fourth harmonic emission isolated using DM5-DM8. A half waveplate (fused silica, air spaced, thickness 0.2 mm × 2 plate) was inserted in the beam path between DM2 and DM3 to change the direction of polarization pararell to that of the fourth harmonic emission. The optical system to generate the third and fifth harmonic emissions simultaneously is shown in Fig. S2A. A photograph of the harmonic generation/separation system is shown in Fig. S2B. The holder of the optical component such as the BBO crystal and the dichroic mirror was mounted on a pair of kinematic bases combined with three magnet pibots (angle resettability 6.36 μrad, KB25/M, Thorlabs). Therefore, the optical component can be quickly replaced and be used without re-adjustments. The output power of the laser was measured by a power meter (PM10X, FieldMate, Coherent). A pair of dielectric mirrors (or aluminum mirrors in the two-color experiment) was used to introduce the laser beam into the MS. The laser beam was focused by a convex lens made of fused silica (focal length 150 mm, SLSQ-25-150P, Sigma-Koki) mounted on a three-dimensional translation stage into a molecular beam in the MS.

### *2.2. Miniature mass analyzer*

Fig. 2 shows the linear-type TOF mass analyzer (width 200 mm, length 160 mm, height 130 mm) that was developed in this study (see the photograph in Fig. S3). A sample was introduced into the

ionization region using a fused-silica capillary that was crossed against the laser beam at a small angle to increase the ionization volume [34]. The capillary was guided with a metal tube supported by an aluminum plate that was heated using a cartridge heater (MCHSSC8-50-V100-W50, Misumi). A ring-type repeller electrode was mounted on a ceramic block attached to the vacuum chamber that was heated from the outside using the cartridge heater. A skimmer-type electrode was used to extract the ion formed by MPI. The ion was further accelerated by a potential applied between the extraction electrode and the flight tube (length 65 mm). The maximum voltage applied to the electrodes was limited to ±5 kV by the MHV connetor used as a high-voltage feedthrough. The ion was separated in the flight tube and was detected by an asssembly of microchannel plates (MCP, F14844-Y002, response time ca. 600 ps, Hamamatsu Photonics). The top panel of the mass analyzer was made of an acryl plate, but was replaced with an aluminum one when the chamber was heated for measuring analytes with low volatility. The vacuum chamber was evacuated through a butterfly valve by a turbomolecular pump (190 L/s, UTM150, Ulvac) followed by a rotary pump (60 L/min, GLD-051, Ulvac). The vacuum pressure was measured by a pirany gage (WP-01, Ulvac) and an ion gage (WIB-G5, Ulvac). A typical vacuum pressure was $4 \times 10^{-3}$ Pa when a sample gas was introduced into the mass analyzer at a rate of 1 mL/min (background pressure, $4 \times 10^{-4}$ Pa).

### *2.3. Analytical system*

Fig. 3 shows a block diagram of the analytical system developed in this study. The signal from the MCP was passed through an amplifier (C5594, bandwidth 1.5 GHz, Hamamatsu Photonics). The time interval between the electronic pulses from the laser (start pulse) and the amplifier (stop pulse) was measured using a time-to-digital converter (TimeHarp 260 NANO, PicoQuant) installed in a personal computer. The signal was accumulated, and a histogram was displayed on a monitor using a solfware program developed in this laboratory.

### *2.4. Gas chromatograph*

As shown in the photograph in Fig. S4, the MS was combined with the GC (6890 N, Agilent Technologies). A 1-μL aliquot of the sample mixture containing 16 PAHs was injected using a splitless mode and was separated by a DB-5ms column (length 30 m, i.d., 0.25 mm, film thickness 0.25 μm). The temperature of the sample injection port was set at 300 °C. Helium was used as a carrier gas at a flow rate of 1 mL/min. The temperature of the column was programed to increase from 40 ºC to 120 ºC at a ramp of 20 ºC/min, then increased to 250 ºC at a rate of 5 ºC/min and was

held for 30 min. The temperature was further increased to 280 ºC at a rate of 5 ºC/min and finally held for 10 min. The temperature of the transfer line to the MS was maintained at 250 ºC.

### *2.5. Reagents*

Chlorobenzene and styrene were purchased from Wako Pure Chemical Industries and pentachlorobenzene from Tokyo Kasei Kogyo. A sample of styrofoam used for packing (manufacturer, unknown) and a polycarbonate film (3-8901, AS ONE Corp.) were used as received. Diisopropyl methylphosphonate (DIMP) and dimethyl methylphosphonate (DMMP) were supplied from Alfa Chemistry and Sigma-Aldrich, respectively. A standard solution of triacetone triperoxide (TATP) prepared at a concentration of 0.1 mg/mL in acetonitorile was obtained from Accu Standard. A sample mixture containing 16 PAHs (Z-013-17, Accu Standard) was diluted with a solvent mixture (1:1) of methanol (Sigma-Aldrich) and dichloromethane (Kanto Chemical).

### *2.6. Sample preparation and introduction into the MS*

Five types of samples were prepared and measured in this study. (1) Neat samples of chlorobenzene, DIMP, and DMMP were placed in a GC vial and gently evaporated at room temperature and was introduced into the MS though a narrow fused-silica capillary (i.d., 0.2 mm, length 1 m, Fused Silica Inertness Tubing, GL Science). The vial was sealed with a vacuum-tight cap, and the analyte was introduced without a diluent gas. (2) a solid sample of pentachlorobenzene in a GC vial was evapolared at room temperature and was introduced into the MS through the capillary using helium as a carrier gas at a flow rate of 1 mL/min. This experiment was performed as a feasibility study for application to a GC detector. (3) styrene (liquid) in a diffusion tube was evaporated and then diluted with nitrogen gas using a standard gas generator (PD-1B, Gastec), which was further mixed with ambient air and was sampled using a fused-silica capillary placed behind the exit port of the standard gas generator to avoid memory effects arising from the analyte adsorbed on the inner surface of the plastic tube (see Fig. S5). A long fused-silica capillary (length 25 m, i.d., 0.53 mm, Fused Silica Inertness Tubing, GL Science) was used to demonstrate on-site real-time monitoring of the sample. (4) a plastic material such as a styrofoam and a polycarbonate film was burned in a flame using a liquid petrolium gas as the fuel and the distal end of the capillary was exposed to the flame to extract the plastic combustion products (typically during 1 s). (5) liquid samples of DIMP and DMMP and a solution of TATP were placed in an evaporating dish that had been rapidly heated on a hot plate to vaporize in the air. The evaporated gas was sampled using the capillary for introduction into the MS (see the photographs shown in Fig. S6).

*2.7. Quantum chemical calculations*

The spectral properties of the molecule were calculated based on density functional theory (DFT). The B3LYP method with a cc-pVDZ basis set was employed to find an optimal geometry. The vertical *IE* was calculated from the difference between the energies of the ground and the ionic states. The lowest one-hundred singlet energies of transition and the oscillator strengths were obtained by time-dependent DFT (TD-DFT). The UV absorption spectrum was displayed using the GaussView 5 software program. The chemical structures and the calculated results are shown in Figs. S7 and S8 and Figs. S9-S28, respectively. In the cases of DIMP and DMMP, the vertical ionization energy and the UV absorption spectrum were calculated at the level of ωB97XD/cc-pVTZ//B3LYP/cc-pVDZ [35].

## 3. Results and discussion

*3.1. Performance evaluation*

*3.1.1. Ionization source*

Table 1 shows the output power of the harmonic emissions generated in this study. The conversion efficiencies achieved from the fundamental (1030 nm) to the third (343 nm), fourth (257 nm), and fifth (206 nm) harmonic emissions were 12, 11, and 0.86%, respectively (the conversion efficiency to the fourth harmonic emission reached 19.7% under optimal conditions, as shown in Figs. S29 and S30), even though the pulse energy of the fundamental emission was limited to 20 μJ. These results were comparable to the efficiencies of 10 and 0.3% for the third (267 nm) and fourth (200 nm) harmonic emissions of a high-power femtosecond TS (800 nm, 35 fs, 1-4 mJ), respectively. The variation in the output power of the fourth harmonic emission was ca. 0.2%. As mentioned above, two harmonic beams can be generated simultaneously using the optical system shown in Fig. 1. The output powers for the third and fourth harmonic emissions can be balanced by tilting the angle of the BBO crystal to change the phase matching condition of the BBO crystal for the third harmonic generation. The two beams emitting at different wavelengths are combined, permitting (1) two single-color experiments to be carried out and then compared by quickly interrupting one of them (2) a two-color experiment using both the beams simultaneously. For example, a molecule can be excited by the third harmonic emission and then subsequently ionized by the fourth harmonic emission. This approach increases flexibility in the ionization scheme and improves selectivity in mass spectrometry.

A variety of compounds can be measured by RE2PI or NR2PI with a minimum excess energy to suppress fragmentation, permitting numerous applications as summarized in Table S1. It should be noted that this system can be used in a pump-and-probe experiment by delaying one of the pulses, i.e., by changing the position of DM2 and DM3 mounted on the same translational stage by the micrometer, to measure a lifetime of the intermediate state.

*3.1.2. Chlorobenzene in a vacuum*

A mass spectrum was obtained for chlorobenzene without using a carrier gas to evaluate the performance of the MS developed in this study. As shown in Fig. 4A, a molecular ion was clearly observed in the mass spectrum, and the fragment ion was nearly completely suppressed at low output powers (5 mW). The mass resolution ($m/\Delta m$) achieved was 670, as shown in Fig. 4B. In TOFMS, the mass resolution is determined by the time resolution ($\Delta t$) of the laser/detector/electronics, the spatial spread ($\Delta x$) of the molecules in the ionization region, and the initial velocity distribution ($\Delta v$) of the ions [36]. The full width at half maximum (FWHM) in the mass spectrum was 1.0 ns, which was larger than the pulse width of the laser (400 fs), the transit time spread of the MCP detector (<100 ps), the response of the amplifier (200 ps; transit time spread <100 ps), and the time resolution of the TCSIC system (250 ps/channel). Then, $\Delta t$ can be neglected in this study. The laser beam was tightly focused into a small spot ($\Delta x$ ~0.01 mm), and the ratio of the flight tube length (65 mm) and $\Delta x$ was 65/0.01 = 6500 which is much larger than the mass resolution of 670 determined. In addition, $\Delta x$ can be compensated for in the two-step acceleration scheme using an extraction electrode; all of the ions at different $\Delta x$ position can reach the detector (placed at the ion focus plane) at the same time by applying an optimal electric potential to the extraction electrode [36]. Therefore, $\Delta x$ can be neglected in this study. It should be noted here that $\Delta v$ is more difficult to decrease in a linear-type TOFMS. The root mean square velocity, $(<u^2>)^{1/2}$, of chlorobenzene ($m$ = 112) at room temperature ($T$ = 300 K) was calculated to be 61 m/s using the equation of $(1/2) \times m<u^2> = (3/2)k_bT$, where $m$ is the weight of a chlorobenzene molecule, $k_b$ is the Boltzmann constant, and $T$ is the absolute temperature. The speed of the ion ($v_i$) was calculated to be 45 mm/μs from the ratio of the flight tube length (65 mm) and the arrival time (1.44 μs) for a signal peak observed at $m/z$ = 112. Accordingly, the ratio of $v_i$ and $\Delta v \approx (<u^2>)^{1/2}$ can be calculated to be (45 mm/μs)/(61 m/s) = 740. As a result, $\Delta v$ would be the main factor that determines the mass resolution in this study. There are two approaches for improving mass resolution, i.e., (1) decreasing $\Delta v$ by supersonic jet expansion of the analyte molecule with a diluent gas into a vacuum (2) increasing $v_i$ by applying a high voltage between the repeller electrode and the flight tube, as recognized from the equation of $V = (1/2) \times (m/e) \times (v_i^2)$ where $V$ is the voltage applied

between the repeller electrode and the flight tube, $m$ is the mass of the ion, and $e$ is the charge. Although $\Delta v$ can be compensated for by using a reflectron-type TOFMS [36], the flight time is increased substantially, making the use of a highly-repetitive laser difficult.

It is known that the two Gaussian peaks can be separated (0.3% overlap) at $1/\Delta m = 1.5$ where $\Delta m$ is the width of the peak in the mass spectrum. The observed value ($1/\Delta m = 670/112 = 6.0$) suggests that the two peaks, $[M]^+$ and $[M+1]^+$, are completely separated. The signal was nearly symmetrical (1.2 times larger for a tail part of the pulse at a signal intensity of 1/10), allowing the isotopomer analysis. Four signal peaks observed at $m/z$ = 112, 113, 114, and 115 can be assigned to molecular ions of the isotopomers of $^{12}C_6H_5{}^{35}Cl^+$, $^{12}C_5{}^{13}CH_5{}^{35}Cl^+$, $^{12}C_6H_5{}^{37}Cl^+$, and $^{12}C_5{}^{13}CH_5{}^{37}Cl^+$, respectively. The intensity distribution of these signals (100:6.4:31:2.3) was nearly identical to that (100:6.6:33:2.2) expected from the natural abundances of $^{12}C$:$^{13}C$ = 100:1.1 and $^{35}Cl$:$^{37}Cl$ = 100:33. The statistical error by shot noise was calculated to be 2.7% = $1/\sqrt{1400}$ for the largest signal at $m/z$ = 112. The flight time of the ions was 1.44 μs, which permits the laser to be operated at <700 kHz. The counting ratio (CR), defined as the number of ions at a specified $m/z$ per laser shot, was 0.012 (= 1400 counts/120 kHz × 1 s) for the largest signal at $m/z$ = 112, suggesting that the signal saturation in TCSIC is negligible under the present conditions.

As shown in Fig. S31, the signal intensity was proportional to the square of the laser output power up to 8 mW (pulse energy <67 nJ = 8 mW/120 kHz), as expected from the model based on RE2PI [37], at which the total counting ratio (TCR), defined as the total number of ions in the mass spectrum per laser shot, appeared on the monitor was 0.80. At larger output powers, the molecular ion that was observed at $m/z$ = 112 tended to saturate and reach the maximum at TCR = 6.2. The fragment ion observed at $m/z$ = 77 ($C_6H_5^+$) appeared and reached the maximum at TCR = 6.0, and the fragment ion at $m/z$ = 51 subsequently appeared, increased more rapidly, and reached a maximum at TCR = 4.3. Thus, the mass spectrum could be measured even at TCR>7 using the time-to-digital converter, although further study will be needed to separate the contributions of the signal saturations arising from TCSIC and MPI. The distribution of the signal intensities for the isotopomers of $^{12}C_6H_5{}^{35}Cl^+$, $^{12}C_5{}^{13}CH_5{}^{35}Cl^+$, $^{12}C_6H_5{}^{37}Cl^+$, and $^{12}C_5{}^{13}CH_5{}^{37}Cl^+$ was measured at different laser powers (5-20 mW) and repetition rates (120-560 kHz), and the results are shown in Fig. S32. When the repetition rate of the laser was changed from 120 kHz to 560 kHz at <10 mW, the shape of the mass spectrum remained unchanged. As expected, the signal intensity decreased in proportion to the repetition rate of the laser, since it is proportional to the repetition rate and to the square of the laser pulse energy [37]. At higher laser powers (20 mW), the mass spectrum was slightly deformed when measured at lower repetition rates (120 kHz, CR = 0.23). In fact, the first signal ($^{12}C_6H_5{}^{35}Cl^+$) was slightly larger and narrower

than the expected ones, which can be attributed to a coincidence of two single-ion pulses (double ion event) in TCSIC. However, such an undesirable effect can be avoided by increasing the repetition rate of the laser, e.g., to 560 kHz (or by decreasing the concentration of the analyte or by loosely focusing the laser beam onto the molecular beam).

When the ordinate scale in the mass spectrum was expanded 50-fold, a broad background signal appeared as a pedestal underneath the sharp peak, as shown in Fig. S33. This undesirable signal became more distinctive when the pumping rate the vacuum chamber was decreased by partially closing the butterfly valve attached on the turbomolecular pump (>0.02 Pa). This background signal could have produced from a collision of an ion against a neutral species such as nitrogen/oxygen remaining in the vacuum chamber. As shown in Fig. S34, the mass spectrum of the background signal measured at 250 mW was comprised of many unknown peaks at $<m/z = 100$. The signals increased with increasing background pressure and can be attributed to contaminants in the vacuum chamber (or in the air). The background signal was considerably smaller at higher *m/z* values. The sensitivity of the MS can be improved by increasing the accumulation time (the maximum value permitted by the software is 10 hr = 36,000 s).

### *3.1.3. Pentachlorobenzene in helium*

Fig. 5A shows the mass spectrum measured for pentachlorobenzene that was introduced into the MS using helium as the carrier gas. A series of isotopomers of the molecular ion consisting of $^{35}Cl/^{37}Cl$ and $^{12}C/^{13}C$ was observed as assigned in Fig. 5B. The signal intensity of the fragment ion was small, although such ions can be increased at high laser powers [38]. The mass resolution was 650, which was slightly smaller than the value obtained uisng chlorobenzene (670). This result can be attributed to the fact that the flight time increases in proportion to the square root of the molecular weight and the spacing in flight time between $[M]^+$ and $[M+1]^+$ decreases at longer flight times.

### *3.1.4. Styrene in air*

Fig. S35 shows the mass spectrum of styrene prepared at 0.1 ppm in nitrogen gas and mixed with ambient air. A molecular ion was observed at $m/z = 104$, in addition to several fragment ions. The limit of detection (LOD) and the lower limit of quantification (LLOQ) were determined by a shot noise (a statistical noise determined by the number of ions detected) and were 0.64 and 7.1 ppb, respectively. The molecular ion signal was slightly broadened at the base of the peak, which can be attributed to the collision of the analyte ion with a neutral species such as nitrogen/oxygen in the diluent gas. This unfavorable result was more distinctive when a fused-silica capillary with a larger

inner diameter was used to increase the flow rate in an effort to improve the sensitivity. Large signals were observed at *m/z* = 18 and 32, which can be assigned to $H_2O$ and $O_2$ in the air, respectively. The ionization energy for these compounds was 12.6 and 12.1 eV in the NIST database, respectively. Therefore, they appeared via non-resonant three-photon ionization (NR3PI) at 257 nm (4.81 eV), which is in contrast to the ionization of styrene, which occurs via RE2PI. Accordingly, the background signal arising from $H_2O$ and $O_2$ in the air could be suppressed by decreasing the photon density on the analyte in the molecular beam.

### *3.2. Applications for on-site real-time monitoring*

#### *3.2.1. Combustion products of polymers*

A styrofoam sample was burned and the constituents in the flame was measured as a feasibility study for the on-site real-time monitoring of polymeric materials. An example of a time course of the mass spectrum is shown in Fig. 6A. It is interesting to note that there are two groups of constituents in the data. One group consists of the components separated in the capillary that was used for sampling, probably due to the adsorption or partition of the analytes on the capillary; the inner surface of the capillary has no stationary phase but is end-capped with an inert material. A series of signals observed at *m/z* = 43, 41, 29, and 28, and 27 can be assigned to the propane/butane used as the fuel for the flame, since the mass fragment pattern is very similar to the NIST data obtained by EIMS [39]. On the other hand, the signals observed at *m/z* = 78 and 92 can be assigned to benzene and toluene, respectively. The signals at *m/z* = 104 and 118 arise from styrene, a monomer of polystyrene, and α-methylstyrene (see the chemical structures in Fig. S7). When compared with the data obtained by "thermally" decomposed products of polystyrene [40], the data obtained by burning a styrofoam was comprised of chemical species with lower molecular weights. This is probably due to the higher temperature of the flame that was used in this study. The other group consists of signals observed continuously at *m/z* = 32, 28, 25, 18, 14, 12, and 1, which can be assigned to $O_2^+$, $N_2^+$, $C_2H^+$, $H_2O^+$, $N^+$ or $CH_2^+$, $C^+$, and $H^+$, respectively. They are likely derived from the constituents in the air and also from the combustion products of the flame. The ionization energies of the related compounds are summarized in Table S2, suggesting RE2PI for the aromatic hydrocarbons, NR3PI for propane/butane, $O_2$, and $H_2O$, and non-resonant four-photon ionization (NR4PI) for $N_2$. Due to a higher ionization energy (15.581 eV), $N_2$ is ionized more inefficiently than $O_2$, even though its natural abundance in air is 80%.

Fig. 6B show a time course for the mass spectrum measured for the combustion products derived

from a polycarbonate film. Signals corresponding to several components such as bisphenol A, styrene, α-methylstyrene, phenol, *p*-cresol, and *p*-vinylphenol can be observed in the data. The ionization energies of the related compounds are summarized in Table S3, suggesting RE2PI for the aromatic hydrocarbons. As demonstrated, polymeric material can readily be determined by burning it and measuring the mass spectrum, providing useful information concerning recycling the polymer material to reduce the amounts of microplastics that are released in the oceans.

*3.2.2. Nerve agent analogs*

Fig. 7 shows the time course for the mass spectrum measured for DIMP, a nerve agent analog, which was vaporized into the atmosphere by heating at 210 °C. As shown in Fig. S36, the fragment pattern below $m/z$ = 140 was very similar to the data obtained by EIMS. However, a molecular ion was observed at $m/z$ = 180, in addition to large fragment ions at $m/z$ = 154 and 165, in the mass spectrum measured by fs-LIMS. Thus, DIMP can be reliably detected in < 1 s by f-LIMS. The *IE* calculated by DFT was 9.93 eV (124.8 nm), suggesting a large excess energy of 4.56 eV via NR3PI at 257 nm (4.83 eV) (see Fig. S26). Therefore, it would be desirable to ionize via NR2PI at shorter wavelengths, e.g., at 206 nm (two-photon energy 12.08 eV) with an excess energy of 2.15 eV or at 206 and 257 nm (two-color two-photon energy 10.87 eV) with an excess energy of 0.94 eV for observing the molecular ion more clearly. It has been reported that a fragment ion ($m/z$ = 123) was observed for DIMP in a supersonic molecular beam by one-photon absorption + two-photon ionization (i.e., 1 + 2 REMPI) at 265.99 nm and a smaller ion ($m/z$ = 43) by 2 + 2 REMPI at 401.97 nm, when a tunable nanosecond laser was used as the ionization source [41]. On the other hand, a molecular ion was observed in the range of 8-12 eV when a single-photon ionization source was used [42,43]. As shown in Fig. S36, a similar result was observed for DMMP, in which a molecular ion was more clearly observed in fs-LIMS than EIMS. Due to the higher *IE* value (10.00 eV in NIST and 10.30 eV in DFT) for DMMP (see Fig. S27), this favorable result can be attributed to a small excess energy of 4.49 eV and the methyl groups in DMMP, which are smaller than the isopropyl groups in DIMP.

*3.2.3. Explosive*

As shown in Fig. S37, the mass spectrum of TATP consisted of large fragment ions in the range of $m/z$ > 80, which was in contrast to the data obtained by EIMS. Therefore, fs-LIMS would be preferred in terms of obtaining a reliable identification. However, the molecular ion was much smaller at 257 nm than that measured at 267 nm [44-46]. The *IE* value calculated by DFT was 8.67-8.88 eV

(142.9-139.7 nm), suggesting NR2PI with a larger excess energy at 257 nm and more efficient fragmentation. An alternative approach for observing a molecular ion would be two-color RE2PI at 206/343 nm (see Fig. S28).

*3.2.4. Applications to GC-MS*

Fig. 8 shows the two-dimensional display of GC-MS measured for a sample mixture containing 16 PAHs. All of the compounds were separated by GC and could be measured by MS. As shown in Fig. S38, the isotopomers of the molecular ion were clearly observed and the fragment ions were suppressed in the mass spectrum that was extracted from the two-dimensional data, at which benzo(a)anthracene appeared. The LOD was 83 fg (LLOQ = 920 fg) at a laser power of 10 mW, which was comparable to the values obtained by EI/quadrupole MS (EI/QMS) and EI/TOFMS. Accordingly, a smaller low-cost Yb laser would be expected to perform sufficiently in applications to trace analysis. The LOD and LLOQ were not determined by the shot noise but by the contaminants remaining in the vacuum chamber. Since the signal intensity increases in proportion to the square of the laser output power in 2PI [36], the signal intensity would increase by 625-fold at 250 mW, providing a calculated LOD of 0.13 fg (LLOQ = 1.4 fg) under the assumption of no background. This value is comparable to the values of 7.5 fg obtained using the third harmonic emission (261 nm, 86 mW) of a TS (784 nm, 900 mW, 1 kHz) and the value of 0.6 fg obtained using the fourth harmonic emission (258 nm, 790 mW) of a high-power picosecond Yb:YAG laser (1031 nm, 4.0 W, 20 kHz) [47]. The background signal could be decreased by introducing helium gas, since it swept out the contaminants in the ionization region. As mentioned above, a variety of wavelengths and combinations thereof can be used for MPI in the present analytical system. For example, the third harmonic emission (3.59 eV) will be useful for RE2PI of benzo(a)pyrene (*IE* = 7.12 eV) [48], a well-known carcinogenic compound, and the background signal will be substantially suppressed, since most organic molecules are not ionized by RE2PI at this wavelength. On the other hand, the third harmonic emission (3.59 eV) will be useful for excitation and the fourth harmonic emission (4.82 eV) for the subsequent ionization of pyrene (*IE* = 7.426 eV) using two-color RE2PI [49]. The fragmentation would then be suppressed by RE2PI with a small excess energy (0.98 = 7.426 - 3.59 - 4.82 eV) [14,50]. For finger-printing identification, the fragmentation can be enhanced by increasing the output power of the fourth harmonic emission (or by focusing the beam more tightly). The time required for recording a mass spectrum can be reduced to 0.1 s, and the MS can then be applied as a detector in GC × GC × TOFMS.

## 4. Conclusion

We report on the development of a miniature mass analyzer for use in combination with a highly-repetitive femtosecond Yb laser and a TCSIC system. A UV pulse (343, 257, 206 nm) was efficiently produced by the harmonic generation of the fundamental pulse (1030 nm) and used as the ionization source. Due to the high repetition rate of the laser, it was possible to obtain a mass spectrum within a short time interval (<1 s), thus permitting the on-site, real-time monitoring of the combustion products appeared by burning, and of nerve agent analogs and the explosive in the air. The developed TOFMS was applied as a GC detector for the comprehensive analysis of PAHs, in which the selectivity can be optimized by selecting the wavelength of the laser being used. Accordingly, this approach has the potential for use in practical trace analysis of various organic compounds in environmental and forensic sciences.

## CRediT authorship contribution statement

**Katsunori Yoshinaga:** Performed the experimental work and designed the mass spectrometer. **Nguyen Van Hao:** Performed the experimental work. **Totaro Imasaka:** Supervision and wrote the draft. **Tomoko Imasaka:** Funding acquisition, supervision, and computational calculations.

## Declaration of competing interest

The authors declare no competing financial interest.

## Acknowledgments

This research was supported by a Grant-in-Aid for Scientific Research from the Japan Society for the Promotion of Science [JSPS KAKENHI Grant Numbers 20H02399] and by the Program of Progress 100 in Kyushu University, The Iwatani Naoji Foundation, 2020 Collaboration Development Fund for Joint Program between National Taiwan Normal University and Kyushu University, Collaboration Research Fund of Nuclear Safety Research & Development Center of Chubu Electric Power Co., Inc., and Heiwa Nakajima Foundation. Quantum chemical calculations were mainly carried out using the computer facilities at the Research Institute for Information Technology, Kyushu University.

## Appendix A. Supplementary data

Supplementary data to this article can be found online at ……

## References


[1] J.H. Gross, Chemical Ionization, In Mass spectrometry, 2nd ed.; Springer-Verlag, Heidelberg, 2004, pp. 341−344.

[2] M. Karas, F. Hillenkamp, Laser desorption ionization of proteins with molecular masses exceeding 10,000 daltons. Anal. Chem. 60 (1988) 2299−2301.

[3] J.B. Fenn, M. Mann, C.K. Meng, S.F. Wong, Whitehouse, C. M. Electrospray ionization for mass spectrometry of large biomolecules. Science 246 (1989) 64−71.

[4] C. Ladavie`re, P.L. Desmazes, F. Delolme, First systematic MALDI/ESI mass spectrometry comparison to characterize polystyrene synthesized by different controlled radical polymerizations. Macromolecules 42 (2009) 70−84.

[5] D.J. Butcher, Vacuum ultraviolet radiation for single-photoionization mass spectrometry: A Review. Microchim. J. 62 (1999) 354−362.

[6] Z. Zhou, H. Guo, F. Qi, Recent developments in synchrotron vacuum ultraviolet photoionization coupled to mass spectrometry. Trends Anal. Chem. 30 (2011) 1400−1409.

[7] J. Kleeblatt, S, Ehlert, J. Holzer, M. Sklorz, J. Rittgen, P. Baumgartel, J.K. Schubert, R. Zimmermann, Investigation of the photoionization properties of pharmaceutically relevant substances by resonance-enhanced multiphoton ionization spectroscopy and single-photon ionization spectroscopy using synchrotron radiation. Appl. Spectrosc. 57 (2013) 860−872.

[8] D.M. Lubman, M.N. Kronick, Mass spectrometry of aromatic molecules with resonance-enhanced multiphoton ionization. Anal. Chem. 54 (1982) 660−665.

[9] U. Boesl, R. Zimmermann, C. Weickhardt, D. Lenoir, D.-W. Schramm, A. Kettrup, E.W. Schlag, Resonance-enhanced multi-photon ionization: A species-selective ion source for analytical time-of-flight mass spectroscopy. Chemosphere 29 (1994) 1429−1440.

[10] Y.-C. Chang, T. Imasaka, Simple pretreatment procedure combined with gas chromatography/multiphoton ionization/mass spectrometry for the analysis of dioxins in soil samples obtained after the Tōhoku earthquake. Anal. Chem. 85 (2013) 349−354.

[11] X. Yang, T. Imasaka, T. Imasaka, Determination of pesticides by gas chromatography combined with mass spectrometry using femtosecond lasers emitting at 267, 400, and 800 nm as the ionization source. Anal. Chem. 90 (2018) 4886−4893.

[12] O. Shitamichi, T. Imasaka, T. Uchimura, T. Imasaka, Multiphoton ionization/mass spectrometry of polybrominated diphenyl ethers. Anal. Methods 3 (2011) 2322−2327.

[13] A. Li, T. Imasaka, T. Imasaka, Optimal laser wavelength for femtosecond ionization of polycyclic aromatic hydrocarbons and their nitrated compounds in mass spectrometry. Anal. Chem. 90 (2018) 2963−2969.

[14] S.L. Madunil, T. Imasaka, T. Imasaka, Suppression of fragmentation in mass spectrometry. Anal. Chem. 92 (2020) 16016−16023.

[15] T. Imasaka, T. Imasaka, Femtosecond ionization mass spectrometry for chromatographic detection, J. Chromatogr. A 1642 (2021) 462023.

[16] N. Reusch, V. Krein, N. Wollscheid, K.-M. Weitzel, Distinction of structural isomers of benzenediamin and difluorobenzene by means of chirped femtosecond laser ionization mass spectrometry. Z. Phys.Chem. 232 (2018) 689−703.

[17] V. Schäfer, K.-M. Weitzel, Qualitative and quantitative distinction of ortho-, meta- and para-fluorotoluene by means of chirped femtosecond laser ionization. Anal. Chem. 92 (2020) 5492−5499.

[18] K.M. Tibbetts, Coherent vibrational and dissociation dynamics of polyatomic radical cations. Chem. Eur. J. 25 (2019) 8431−8439.

[19] D. Ampadu-Boateng, G.L. Gutsev, P. Jena, K.M. Tibbetts, Dissociation dynamics of 3- and 4-nitrotoluene radical cations: Coherently driven C-$NO_2$ bond homolysis. J. Chem. Phys. 148 (2018) 134305.

[20] S.L. McPherson, J.M. Shusterman, H.A. López Peña, D.A. Boateng, K.M. Tibbetts, Quantitative analysis of nitrotoluene isomer mixtures using femtosecond time-resolved mass spectrometry. https://doi.org/10.1021/acs.analchem.1c02245.

[21] Y.S. Shimma, H. Nagao, J. Aoki, K. Takahashi, S. Miki, M. Toyoda, Miniaturized high-resolution time-of-flight mass spectrometer MULTUM-S II with an infinite flight path. Anal. Chem. 82 (2010) 8456−8463.

[22] T.J. Cornish, R.J. Cotter, High-order kinetic energy focusing in an end cap reflectron time-of-flight mass spectrometer. Anal. Chem. 69 (1997) 4615−4618.

[23] R.J. Cotter, C. Fancher, T.J. Cornish, Miniaturized time-of-flight mass spectrometer for peptide and oligonucleotide analysis. J. Mass Spectrom. 34 (1999) 1368−1372.

[24] R.J. Cotter, The new time-of-flight mass spectrometry. Anal. Chem. 71 (1999) 445A−451A.

[25] M.C. Prieto, V.V. Kovtoun, R.J. Cotter, Miniaturized liner time-of-flight mass spectrometer with pulsed extraction. J. Mass Spectrom. 37 (2002) 1158−1162.

[26] R.J. Cotter, R.D. English, B. Warscheid, A. Hardy, B.D. Gardner, Miniaturized time-of-flight mass spectrometers for bioagent detection and identification. J. Mass Spectrom. Soc. Jpn. 51 (2003) 36−41.

[27] R.D. English, B. Warscheid, C. Fenselau, R.J. Cotter, Bacillus spore identification via proteolytic peptide mapping with a miniaturized MALDI TOF mass spectrometer. Anal. Chem. 75 (2003) 6886−6892.

[28] U. Rohner, J.A. Whitby, P. Wurz, Highly miniaturized laser ablation time-of-flight mass spectrometer for a planetary rover. Rev. Sci. Instrum. 75 (2004) 1314−1322.

[29] S.A. Getty, W.B. Brinckerhoff, T. Cornish, S. Ecelberger, M. Floyd, Compact two-step laser time-of-flight mass spectrometer for in situ analyses of aromatic organics and planetary missions. Rapid Commun. Mass Spectrum. 26 (2012) 2786−2790.

[30] G.B. Baptista, A. Brunelle, P. Chaurand, S. Della-Negra, J. Depauw, Y. Le Beyec, Ion counting and ion intensity measurements in time-of-flight mass spectrometry. Application to matrix-assisted laser desorption. Rapid Commun. Mass Spectrom. 5 (1991) 632−637.

[31] T. Onoda, G. Saito, T. Imasaka, Scheme for collinear ionization in supersonic jet/multiphoton ionization/time-of-flight mass spectrometry. Anal. Chim. Acta 412 (2000) 213−219.

[32] G. Saito, T. Imasaka, A digital ion counting technique for noise reduction in supersonic jet/multiphoton ionization/time-of-flight mass spectrometry. Anal. Sci. 15 (1999) 1273−1275.

[33] T. Ju, K. Yoshinaga, T. Imasaka, H. Nakamura, T. Imasaka, Time-correlated single ion counting mass spectrometer with long and short time-of-flight tubes and an evaluation of its performance for use in trace analysis of allergenic substances. Anal. Sci. 36 (2020) 539−543.

[34] T. Matsui, T. Imasaka, Signal enhancement by crossing the sample flow at a small-angle against the laser beam in multiphoton ionization mass spectrometry. Anal. Sci. 30 (2014) 445–449.

[35] R. Bauernschmitt, R. Ahlrichs, Treatment of electronic excitations within the adiabatic approximation of time dependent density functional theory. Chem. Phys. Lett. 256 (1996) 454–464.

[36] R.J. Cotter, Time-of-flight mass spectrometry: Instrumentation and applications in biological research, American Chemical Society, Washington, D.C., 1997.

[37] S.L. Madunil, T. Imasaka, T. Imasaka, Resonant and non-resonant femtosecond ionization mass spectrometry of organochlorine pesticides. Analyst 145 (2020) 777–783.

[38] H. Kouno, T. Imasaka, The efficiencies of resonant and nonresonant multiphoton ionization in the femtosecond region. Analyst 141 (2016) 5274−5280.

[39] National Institute of Standards and Technology, https://webbook.nist.gov/cgi/cbook.cgi?ID=C106978&Units=SI&Mask=200#Mass-Spec

[40] T. Imasaka, M. Hozumi, N. Ishibashi, Supersonic jet spectrometry of chemical species resulting from thermal decomposition of polystyrene and polycarbonate. Anal. Chem. 64 (1992) 2206−2209.

[41] J.A. Syage, J.E. Pollard, R.B. Cohen, Ultrasensitive detection of atmospheric constituents by supersonic molecular beam, multiphoton ionization, mass spectrometry. Anal. Chem. 26 (1987) 3516−3520.

[42] J.A. Syage, M.A. Hanning-Lee, K.A. Hanold, A man-portable, photoionization time-of-flight mass spectrometer. Field Anal. Chem. Tech. 4 (2000) 204−215.

[43] J.A. Syage, B.J. Nies, M.D. Evans, K.A. Hanold, Field-portable, high-speed GC/TOMFMS. J. Am. Soc. Mass Spectrom. 12 (2001) 648−655.

[44] S. Yamaguchi, T. Uchimura, T. Imasaka, T. Imasaka, Gas chromatography/time-of-flight mass spectrometry of triacetone triperoxide based on femtosecond laser ionization. Rapid Commun. Mass Spectrom. 23 (2009) 3101−3106.

[45] R. Ezoe, T. Imasaka, T. Imasaka, Determination of triacetone triperoxide using ultraviolet femtosecond multiphoton ionization time-of-flight mass spectrometry. Anal. Chim. Acta 853 (2015) 508−513.

[46] A. Hamachi, T. Okuno, T. Imasaka, Y. Kida, T. Imasaka, Resonant and nonresonant multiphoton ionization processes in the mass spectrometry of explosives. Anal. Chem. 87 (2015) 3027−3031.

[47] T. Matsui, K. Fukazawa, M. Fujimoto, T. Imasaka, Analysis of persistent organic pollutants at sub-femtogram levels using a high-power picosecond laser in gas chromatography/multiphoton ionization/time-of-flight mass spectrometry. Anal. Sci. 28 (2012) 445−450.

[48] National Institute of Standards and Technology, https://webbook.nist.gov/cgi/cbook.cgi?ID=C50328&Units=SI&Mask=20#Ion-Energetics

[49] National Institute of Standards and Technology, https://webbook.nist.gov/cgi/cbook.cgi?ID=C129000&Units=SI&Mask=20#Ion-Energetics

[50] S. Shibuta, T. Imasaka, T. Imasaka, Determination of fragrance allergens by ultraviolet femtosecond laser ionization mass spectrometry. Anal. Chem. 88 (2016) 10693−10700.

**Table 1.**
Output power of the harmonic emissions

| Method | THG (mW) | FHG (mW) | FIHG (mW) |
|---|---|---|---|
| 1 | 251 | | |
| 2 | | 225 | |
| 3 | | | 18 |
| 4 | 130[a] | 130[a] | |
| 5 | | 132 | 18 |

[a] The angle of the BBO crystal was optimized to provide the same output powers in THG and FHG. Laser power, 2.1 W; pulse repetition rate, 120 kHz.

**Figure captions**

Fig. 1. Optical configuration of the harmonic generator. (A) the third (THG, right) and fourth (FHG, left) harmonic generators (B) the fourth (FHG, right) and fifth (FIHG, left) harmonic generators. DM, dichroic mirror.

Fig. 2. Construction of the miniature mass analyzer.

Fig. 3. Block diagram of the analytical system.

Fig. 4. Mass spectrum of chlorobenzene. (A) total view (B) expanded view. Laser power, 5 mW; accumulation time, 10 s. Applied voltage; repeller electrode, +5.0 kV; extraction electrode, +0.17 kV; flight tube, -1 kV. The assignments of the peaks are shown in the figure. $M^+$, molecular ion.

Fig. 5. Mass spectrum of pentachlorobenzene. (A) total view (B) expanded view. Laser power, 10 mW; accumulation time, 10 s. Applied voltage; repeller electrode, +5.0 kV; extraction electrode, +1.2 kV; flight tube, -1.8 kV. The assignments of the peaks are shown in the figure. $M^+$, molecular ion.

Fig. 6. Time course for the mass spectrum measured for combustion products derived from (A) styrofoam (B) polycarbonate film. The origin ($t = 0$) was determined as the time when the first signal appeared. (A) (a) fuel (propane/butane); $CH_3$-$CH_2$-$CH_2^+$ ($m/z$ = 43), $CH_2$=CH-$CH_2^+$ (41), $CH_3$-$CH_2^+$ (29), $CH_2$=$CH_2^+$ (28), $CH_2$=$CH^+$ (27) (b) benzene (78) (c) toluene (92) (d) styrene (104) (e) α-methylstyrene (118) (f) fragments (g) fuel (h) $O_2^+$ (32) (i) $N_2^+$ (28) (j) C≡$CH^+$ (25) (k) $H_2O^+$ (18) (l) $N^+$ or $CH_2^+$ (14) (m) $C^+$ (12) (n) $H^+$ (1). The signals arising from (d) and (e) appeared several times, which would arise from isomers or multiple sampling in the flame. (B) (a) bisphenol A (228) (b) styrene (104) (c) α-methylstyrene (118) (d) phenol (94) (e) *p*-cresol (108) (f) *p*-vinylphenol (120) (g) $O_2^+$ (32) (h) $N_2^+$ (28) (i) C≡$CH^+$ (25) (j) $H_2O^+$ (18) (k) $C^+$ (12), (l) $C^{2+}$ (6) (n) $H^+$ (1). Accumulation time, 1 s.

Fig. 7. Time course for the mass spectrum measured for DIMP vaporized in an evaporation dish that was rapidly heated to 210 °C. The origin ($t = 0$) was determined as the time when the first signal appeared. Accumulation time, 1 s. The mass spectrum of DIMP vaporized in a GC vial is shown in the right hand side of the figure.

Fig. 8. Two-dimensional display of GC-MS measured for a sample mixture containing 16 PAHs specified by NIST. 1 naphthalene (Mw = 128), 2 acenaphthylene (152), 3 acenaphthene (154), 4 fluorene (166), 5 phenanthrene (178), 6 anthracene (178), 7 fluoranthene (202), 8 pyrene (202), 9 benzo[a]anthracene (228), 10 chrysene (228), 11 benzo[b]fluoranthene (252), 12 benzo[k]fluoranthene (252), 13 benzo[a]pyrene (252), 14 indeno[1,2,3-cd]pyrene (276), 15

dibenzo[a,h]anthracene (278), 16 benzo[ghi]perylene (276). Sample concentration, 0.1 ppm for each component; laser output power, 10 mW.

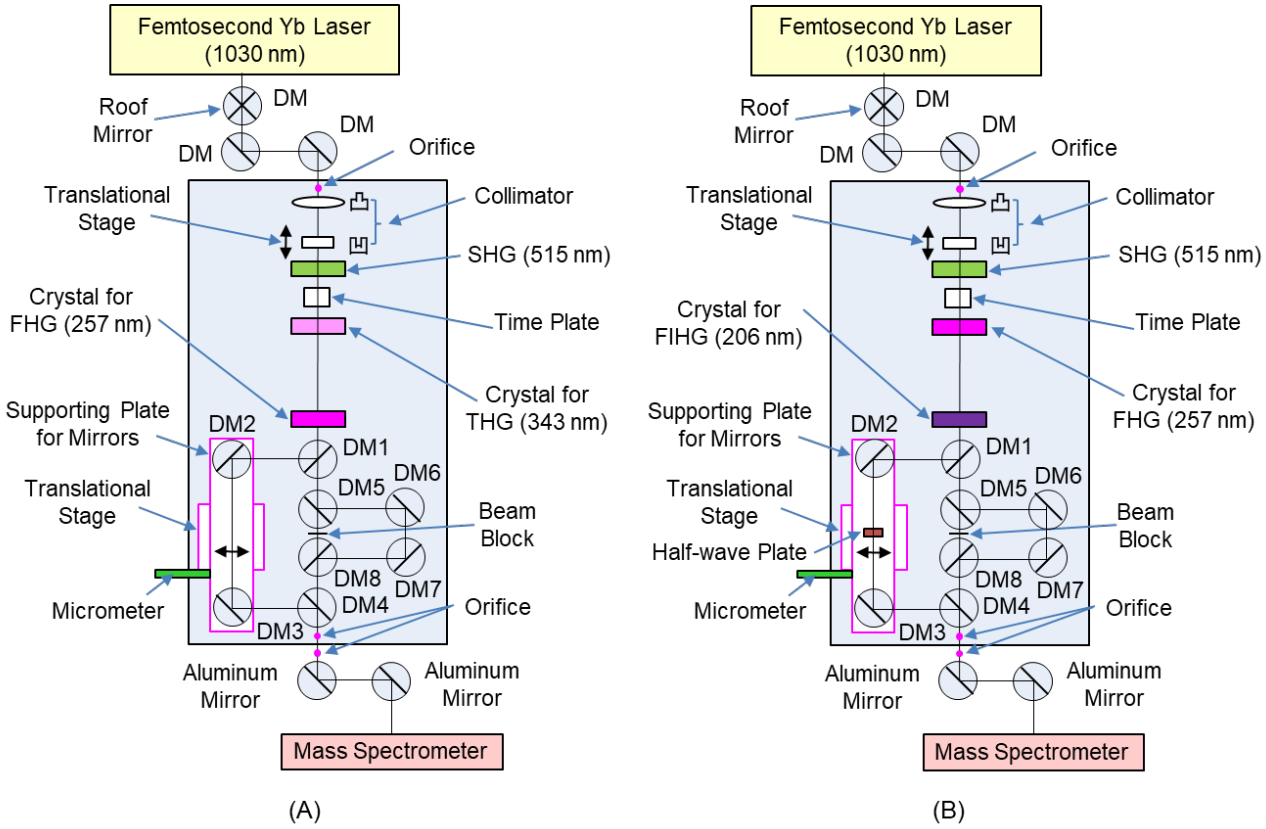


Fig. 1 K. Yoshinaga, et al.

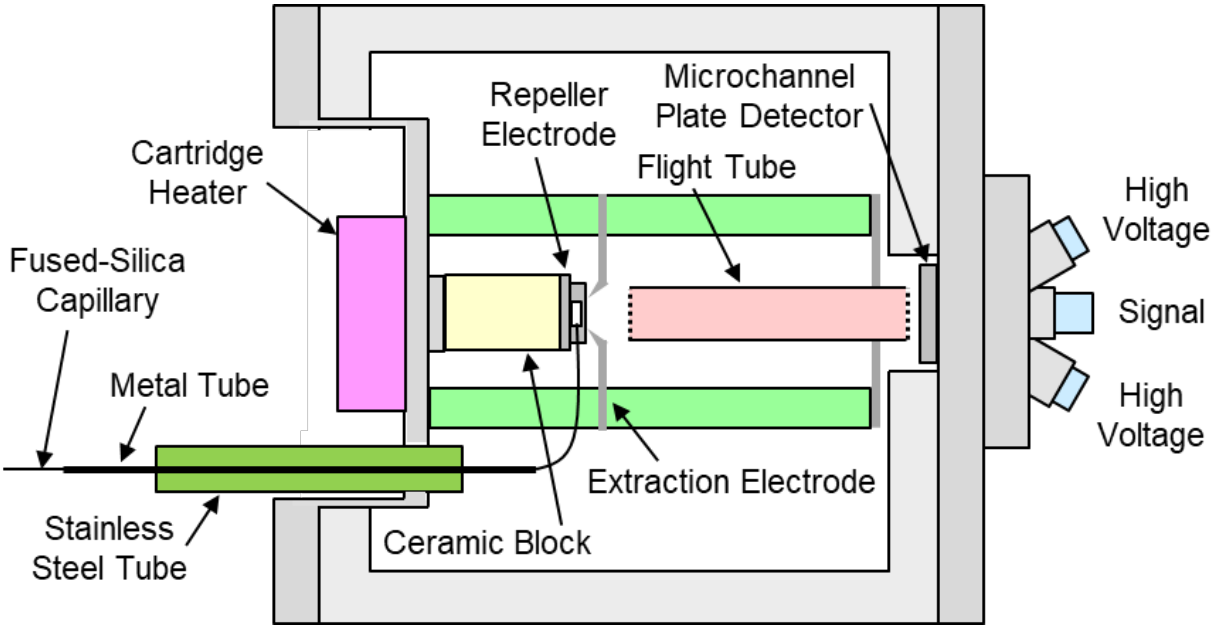


Fig. 2 K. Yoshinaga, et al.

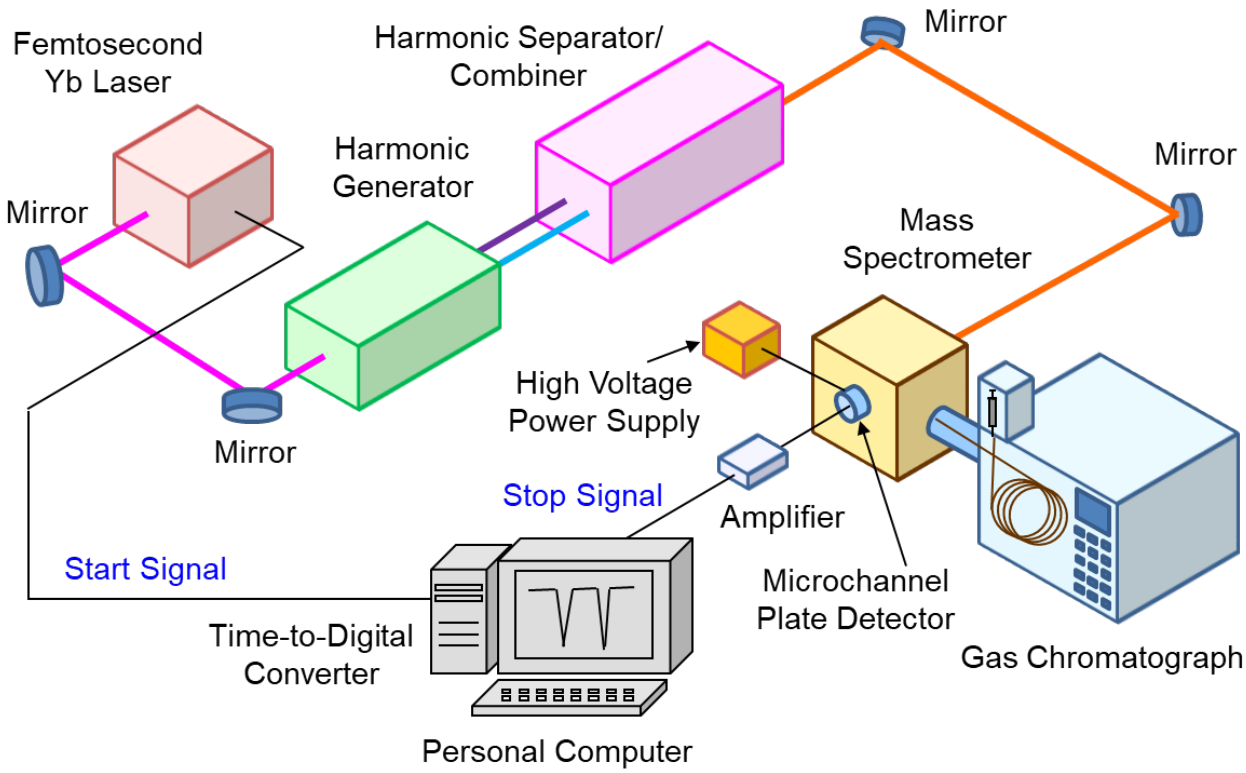


Fig. 3 K. Yoshinaga, et al.

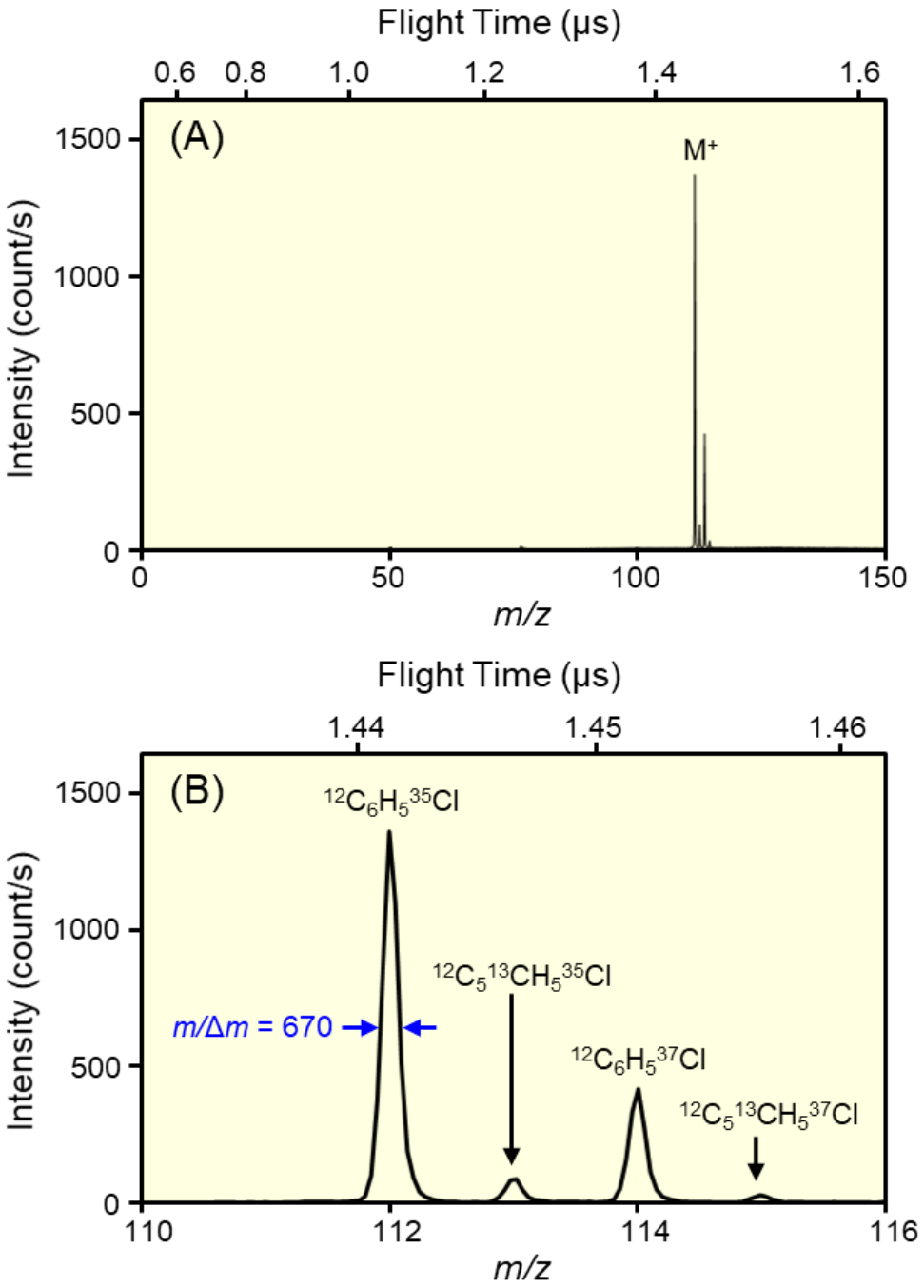


Fig. 4 K. Yoshinaga, et al.

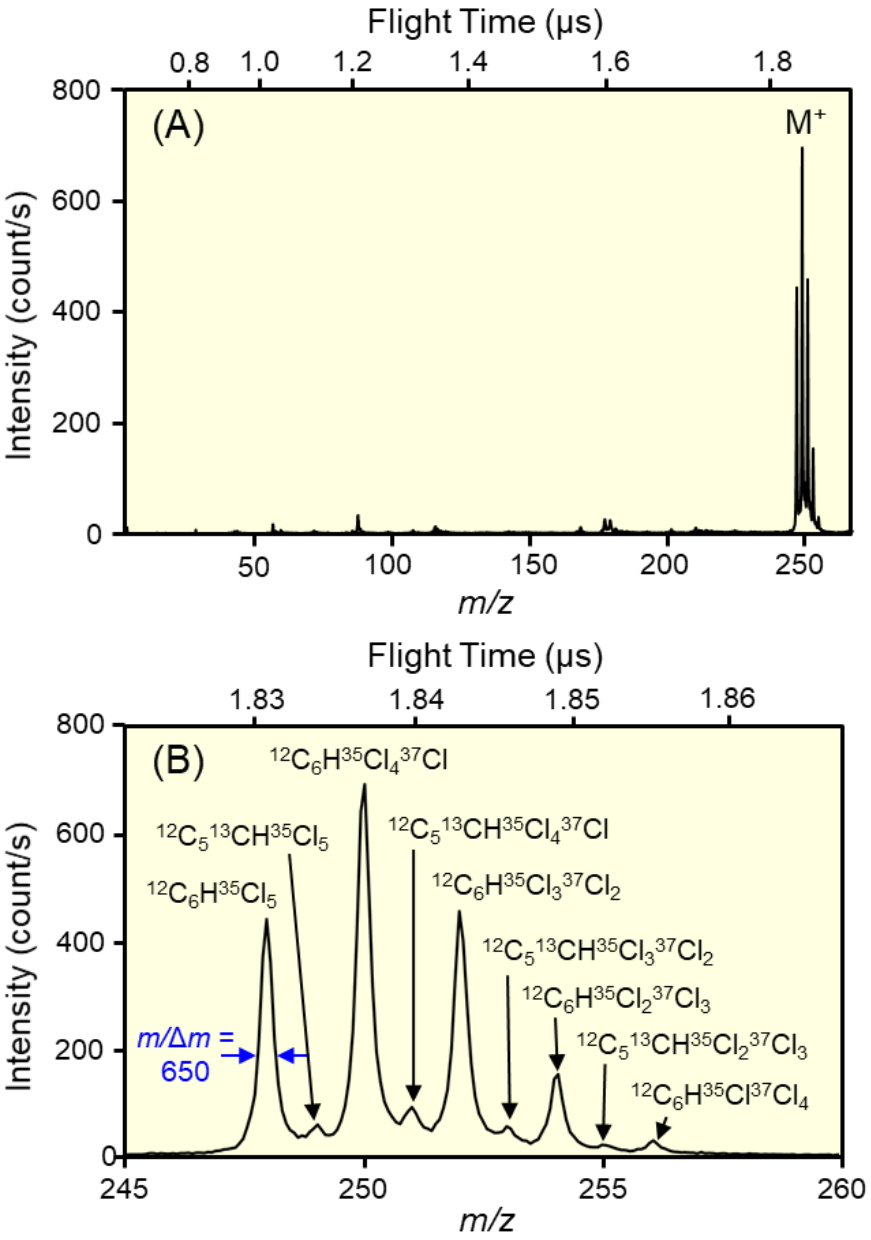


Fig. 5 K. Yoshinaga, et al.

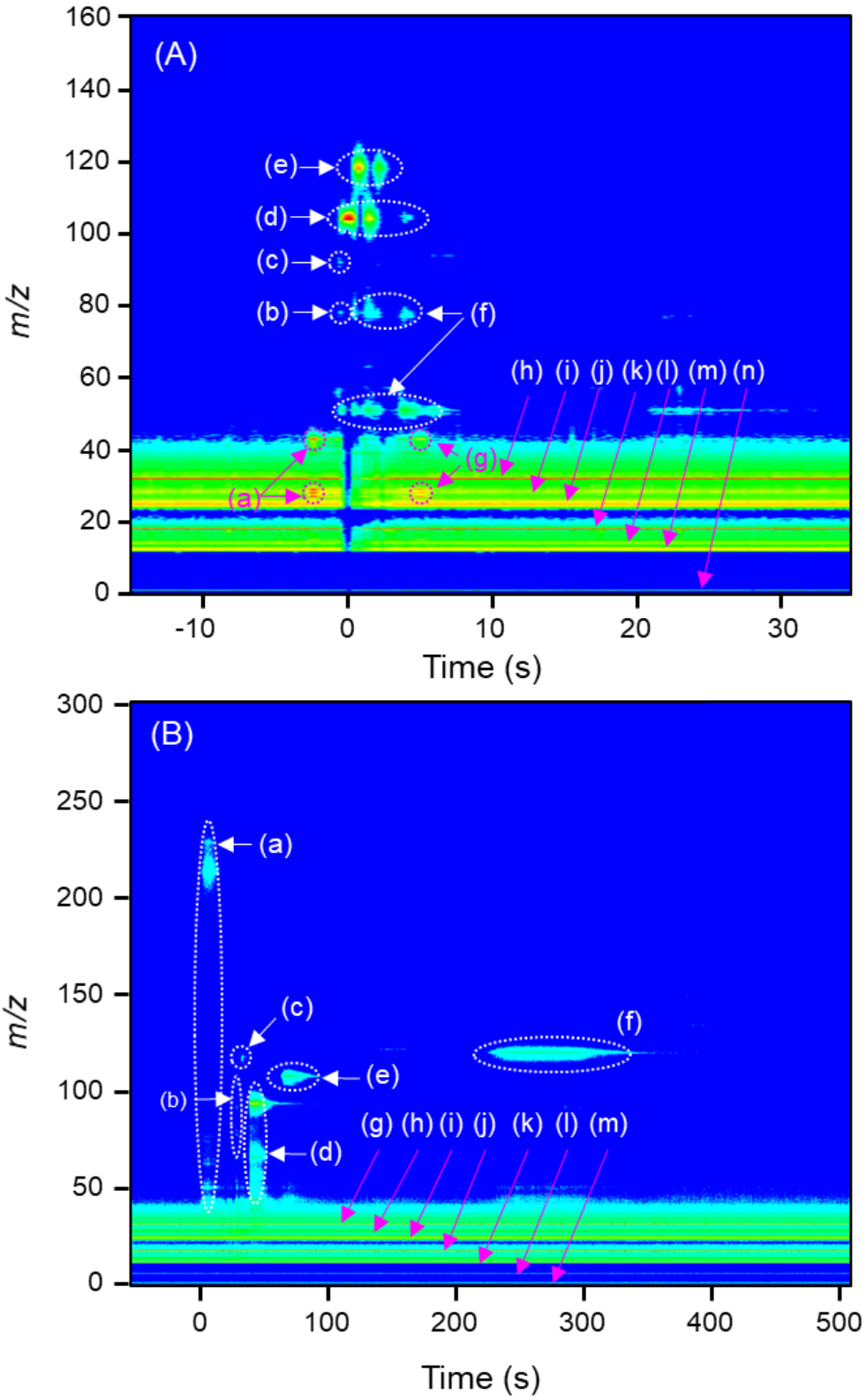


Fig. 6 K. Yoshinaga, et al.

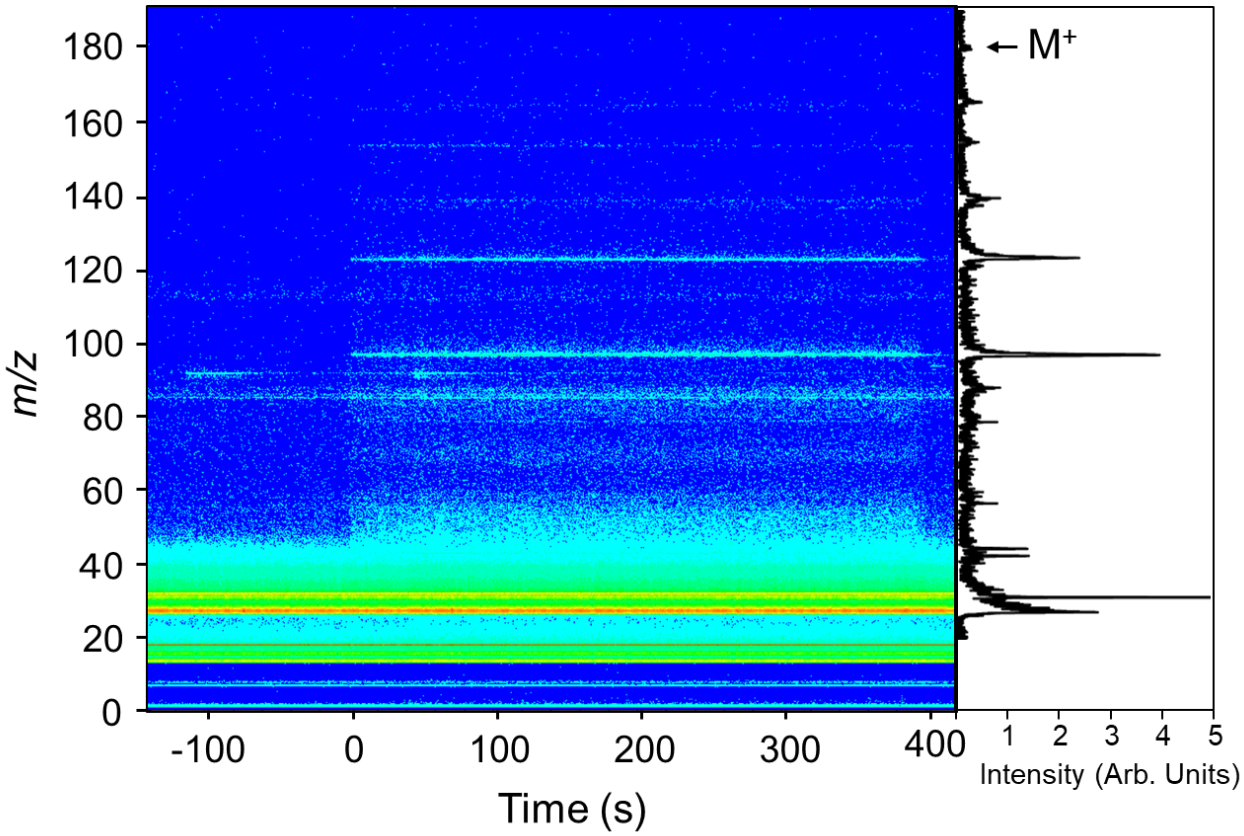


Fig. 7 K. Yoshinaga, et al.

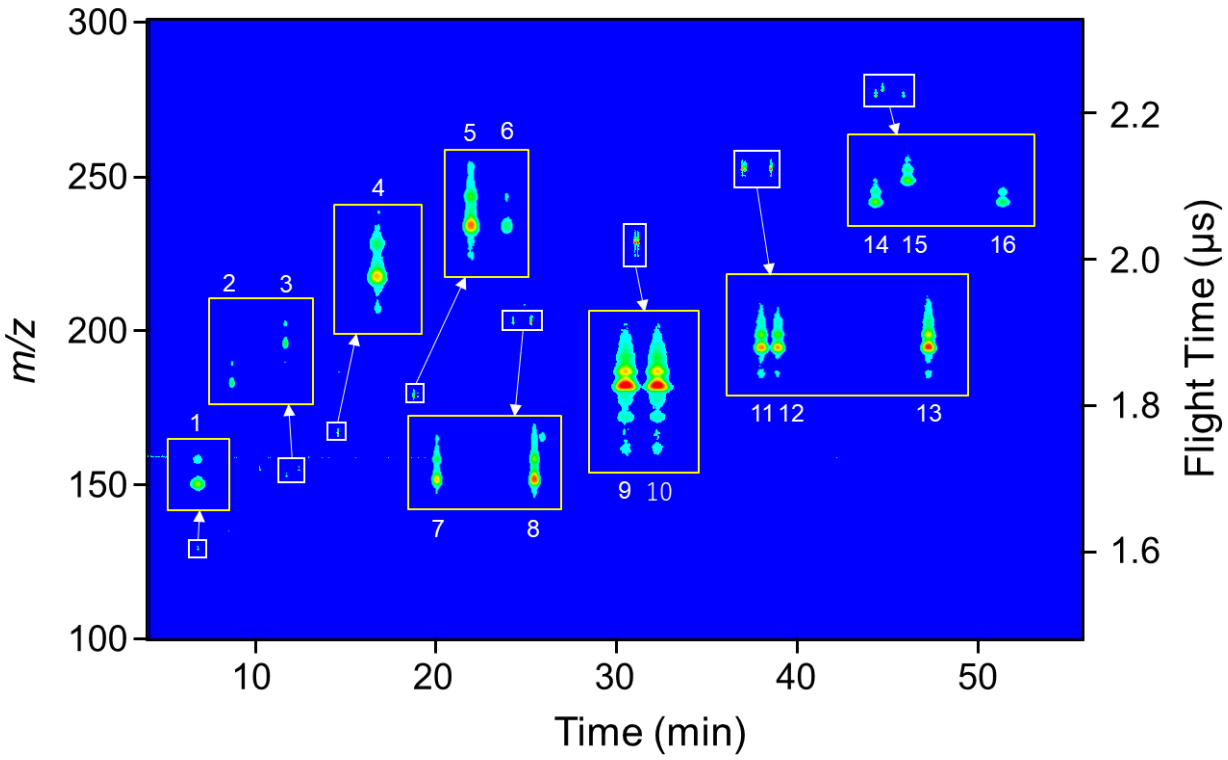


Fig. 8 K. Yoshinaga, et al.